$\beta\nu$-Correlation Analysis: A Modified Two-Dimensional Infrared Correlation Method for Determining Relative Rates of Intensity Change

Douglas L. Elmore and Richard A. Dluhy*

University of Georgia, Department of Chemistry, Athens, Georgia 30602-2556

Received: April 18, 2001; In Final Form: July 24, 2001

A modified two-dimensional infrared (2D IR) correlation method called $\beta\nu$ correlation analysis is introduced for quantitatively determining the relative rates of intensity change and the degree of coherence between intensity variations in a discrete set of dynamic spectra. In a $\beta\nu$ correlation analysis, a mathematical cross correlation is performed between a set of n spectra undergoing some dynamic intensity variation, i.e. $f(\nu, n)$, against a simple mathematical function. In the present case this is a sine function. Correlation intensities are a function of the phase angle (β) of the sinusoidal function and the spectral frequency (ν). The maximum positive correlation intensity will be observed at one point in the asynchronous (β,ν) correlation plot for the range $360° > \beta \geq 0°$. This point is used to define a new parameter, the effective phase angle, β_e, of $f(\nu, n)$, where β_e is simply equal to $\beta + 90°$. In graphical terms, β_e is the point of maximum positive correlation intensity in the asynchronous β vs. ν plot. The β_e value quantitatively reveals the relative rates of change and the degree of coherence between the signal variations in a set of dynamic spectra. Some other desirable properties of $\beta\nu$ correlation analysis include: (1) $\beta\nu$ correlation plots are relatively easy to calculate in that they require no Fourier transformations; (2) the effective phase angle, β_e, is a direct result of the correlation analysis, therefore no additional calculations are required; (3) in appropriate situations β_e values from different experiments may be compared; and (4) noise is observed at a lower level in a $\beta\nu$ correlation plot than the standard 2D IR maps. In this article, simple β_e-relative rate models are introduced, and model calculations are used to help determine the level of uncertainty that can be expected in the β_e values for a set of simulated dynamic spectra. Finally, an application of $\beta\nu$ correlation analysis to the solid−solid-phase transition ("rotator" transition) of *n*-nonadecane (*n*-$C_{19}H_{40}$) is presented.

Introduction

Two-dimensional infrared correlation spectroscopy (2D IR) is a powerful mathematical technique for obtaining information that may be overlooked in conventional IR spectra.[1−5] Many researchers have exploited 2D IR's ability to provide enhanced resolution, simplify complex spectra, identify intermolecular and intramolecular interactions and facilitate band assignments,[6−11] whereas a smaller number of researchers have exploited 2D IR's ability to establish temporal relationships.[12−15] Furthermore, a variety of studies have appeared in the literature in which a heterospectral cross correlation was performed on spectral variations collected from two different spectroscopic techniques.[16−19] However, to our knowledge, no 2D IR correlation analysis has been described in which a spectral variation was cross-correlated with a purely mathematical function. In this paper, we present a modified 2D IR correlation method, which we call $\beta\nu$ correlation analysis, that involves the correlation of spectral variations with a simple sinusoidal function. We will show how $\beta\nu$ correlation analysis can be used to quantitatively determine the relative rates of change (i.e., the temporal relationships) and the degree of coherence between the intensity variations in a discrete set of dynamic spectra.

In general, when the intensity of infrared bands in a set of dynamic spectra vary according to a pure sinusoidal waveform, their temporal relationships or relative rates of change can be determined from the signs of the synchronous and asynchronous cross-peaks in the corresponding 2D IR plots. This is done using a set of rules that have previously been defined.[1] These rules are derived from the phase relationships of the dynamic IR signals and simply restate the fact that the signs of the cross-peaks are determined by the phase angle or phase lag between the two dynamic IR signals. If known, the actual value of the phase angle can be used to quantitatively determine the temporal relationship or describe the degree of coherence between two sinusoidal signal variations.[1,4,20−27] The phase angle, β, between two sinusoidal signal variations is formally defined using eq 1

$$\beta = \tan^{-1}\left(\frac{\Psi}{\Phi}\right) \tag{1}$$

where Φ represents the synchronous correlation intensity and Ψ represents the asynchronous correlation intensity for two independent frequencies (ν_1, ν_2). The mathematical functions that define both Ψ and Φ have been previously presented.[1]

Conversely, in cases where two band intensities vary according to some arbitrary nonsinusoidal waveform, the phase angle can be determined only by methods that require a great deal of computational difficulty.[4,22] The goal of this paper is to introduce a simplified methodology that seeks to avoid the computational difficulties of these exact methods, but still provides a more quantitative approach to describe temporal relationships than simply relying on the signs of cross-peaks. This new method introduces a parameter called the effective phase angle, β_e, that seeks to approximately describe the relative relationship between

* To whom correspondence should be addressed. Office: (706) 542-1950 fax: (706) 542-9454 E-mail: dluhy@chem.uga.edu.

10.1021/jp0114485 CCC: $20.00
Published on Web 10/12/2001

the two signal variations. Like the formally defined phase angle of eq 1, the β_e values can be used to establish both the temporal relationships of dynamic IR signals and to quantitatively determine the degree of coherence between two signal variations. However, unlike true phase angles, β_e values can be easily determined for any signal variation regardless of its waveform. The β_e values are determined by a method that we call $\beta\nu$ correlation analysis, which is introduced in this paper.

Materials and Method

Synthetic Spectra. Synthetic spectra were calculated using an Array Basic program written in our laboratory for the GRAMS/32 (Galactic Industries Corp., Salem, N. H.) environment (R. Dluhy, unpublished). All synthetic spectra were calculated using Lorentzian band shapes with a resolution of 1 cm^{-1}. Full widths at half-maximal peak intensity for the synthetic band shapes were either 5 cm^{-1} for well-resolved peaks or 20 cm^{-1} for overlapped peaks. No additional noise was added to the synthetic spectra.

Calculation of 2D IR Correlation Spectra. The 2D IR synchronous and asynchronous spectra were calculated using the Array Basic program "KG2D" written for GRAMS/32 and generously provided by Professor Yukihiro Ozaki of Kwansei-Gakuin University, Nishinomiya, Japan. This program uses the most recent mathematical formalism in which a Hilbert transform is utilized for calculating the asynchronous spectrum.[28] In all cases, the average spectrum was subtracted from each spectrum to produce a set of dynamic IR spectra. The dynamic spectra were then used in the correlation analysis. The synchronous spectrum, $\Phi(\nu_1,\nu_2)$, and the asynchronous spectrum, $\Psi(\nu_1,\nu_2)$, were calculated using eqs 2 and 3

$$\Phi(\nu_1,\nu_2) = \frac{1}{N-1}\sum_{j=0}^{N-1} y(\nu_1,n_j)\cdot y(\nu_2,n_j) \qquad (2)$$

$$\Psi(\nu_1,\nu_2) = \frac{1}{N-1}\sum_{j=0}^{N-1} y(\nu_1,n_j)\cdot \sum_{k=0}^{N-1} M_{jk}\cdot y(\nu_2,n_k) \qquad (3)$$

In eqs 2 and 3, ν_1 and ν_2 represent two independent frequencies, n_j represents the number of the spectrum in the ordered sequence where the first spectrum number is zero, N represents the total number of spectra used in the calculation, and M_{jk} is the Hilbert transform matrix, which is defined in eq 4

$$M_{jk} = \begin{cases} 0 & \text{if } j = k \\ \dfrac{1}{\pi(k-j)} & \text{otherwise} \end{cases} \qquad (4)$$

***n*-Nonadecane Phase Transition Experiment.** *n*-Nonadecane (n-$C_{19}H_{40}$) was obtained from Fluka Chemical Corp. (Ronkonkoma, NY) at 99.8 + % stated purity as verified by gas chromatography. Samples for infrared measurement were prepared as thin films between two KBr windows with a 15 μm Teflon spacer. The temperature of the sample was controlled with a thermostated cell mount. Infrared spectra were measured at 2 cm^{-1} resolution with a Bruker Equinox 55 Fourier transform infrared spectrometer (Bruker, Billerica, MA) equipped with a DTGS detector. Each spectrum was collected with one scan, apodized with a medium Beer-Norton function and Fourier transformed with two levels of zero filling. The spectra were continuously collected at a rate of one single scan per five seconds as the sample was heated from ~18 °C to ~23 °C. Eleven IR spectra, each comprising a single scan, which represented the first half of the intensity change were used in the correlation analysis. Frequencies and bandwidths (full-width at half-maximum, fwhm) were determined using the GRAMS/32 program.

Results and Discussion

I. Determination of Relative Rates Using Conventional 2D IR Correlation Analysis. The relative temporal relationship between two spectral bands in a set of dynamically varying spectra can currently be determined using 2D IR correlation analysis. The conventions governing relative rates were first described by I. Noda in 1990 and are now commonly referred to as "Noda's rules"; these relationships are presented in Reference 1. Briefly, by noting the sign of the cross-peaks at coordinate (ν_1,ν_2) in the 2D synchronous and asynchronous correlation plots, Noda's rules can be used to determine the order in which the events occur at ν_1 and ν_2 in a set of dynamic spectra. Noda's rules were first developed for the case where the two correlated signals vary with the same waveform; in this case, the meaning of these relationships is most easily understood and justified. However, when the two signals ν_1 and ν_2 vary as two independent mathematical forms, the situation becomes more complicated. This is the situation we wish to explore in the current article.

Note: In this manuscript, all temporal relationships are determined by cross-correlating the "dynamic" IR spectra, not the initially measured, time-resolved spectra. A set of dynamic spectra is a produced by subtracting the mean spectrum from each spectrum in the set of time-resolved spectra. Therefore, the phrase "dynamic signal variation" refers to a change in IR band intensity in the set of dynamic spectra.

Example of The Use of 2D IR to Determine Relative Rates. Consider a case in which 11 IR spectra are collected sequentially, but the intensities at two independent wavenumbers ν_1 and ν_2 vary as two completely different independent functions as the sequence progresses. The intensity variations at ν_1 and ν_2 of spectrum n in the sequence are described by the two functions $f(\nu_1,n)$ and $f(\nu_2,n)$, whose plots are presented in Figure 1A. Note that $f(\nu_1,n)$ and $f(\nu_2,n)$ do not vary as the same waveform or Fourier series differing only by phase angle, but rather have completely different mathematical forms. In the case illustrated in Figure 1A, $f(\nu_1,n)$ varies in a two-step linear fashion, whereas $f(\nu_2,n)$ varies as a partial sine function. In this situation, the meaning of Noda's rules becomes less intuitive; i.e., the phase angles of $f(\nu_1,n)$ and $f(\nu_2,n)$ are not the same for their different Fourier frequency components. However, if the two functions are considered as rough approximations of two sine functions at approximately $^1/_4$ of a full cycle with significantly different phase angles, Noda's rules are more easily understood. That is, we need not calculate true phase angles at different Fourier frequencies to understand why the rules work. Intuitively, from Figure 1A, we can say that $f(\nu_1,n)$ leads and $f(\nu_2,n)$ lags.

Figure 1B illustrates this case with simulated absorption bands. Two well-resolved peaks at 1000 and 900 cm^{-1} were simulated with Lorentzian band shapes having a fwhm of 20 cm^{-1} and a resolution of 1 cm^{-1}. From Figure 1B, it can be seen that the intensities of spectral bands ν_1 and ν_2 vary according to the functions $f(\nu_1,n)$ and $f(\nu_2,n)$ as the spectrum sequence progresses. When a cross correlation is performed on these two signal variations a positive cross-peak is observed in the synchronous map at (ν_1,ν_2) and positive cross-peak is observed in the asynchronous plot at (ν_1,ν_2). The respective 2D IR synchronous and asynchronous correlation maps are illustrated in Figure 1C. In this case, according to Noda's rules,

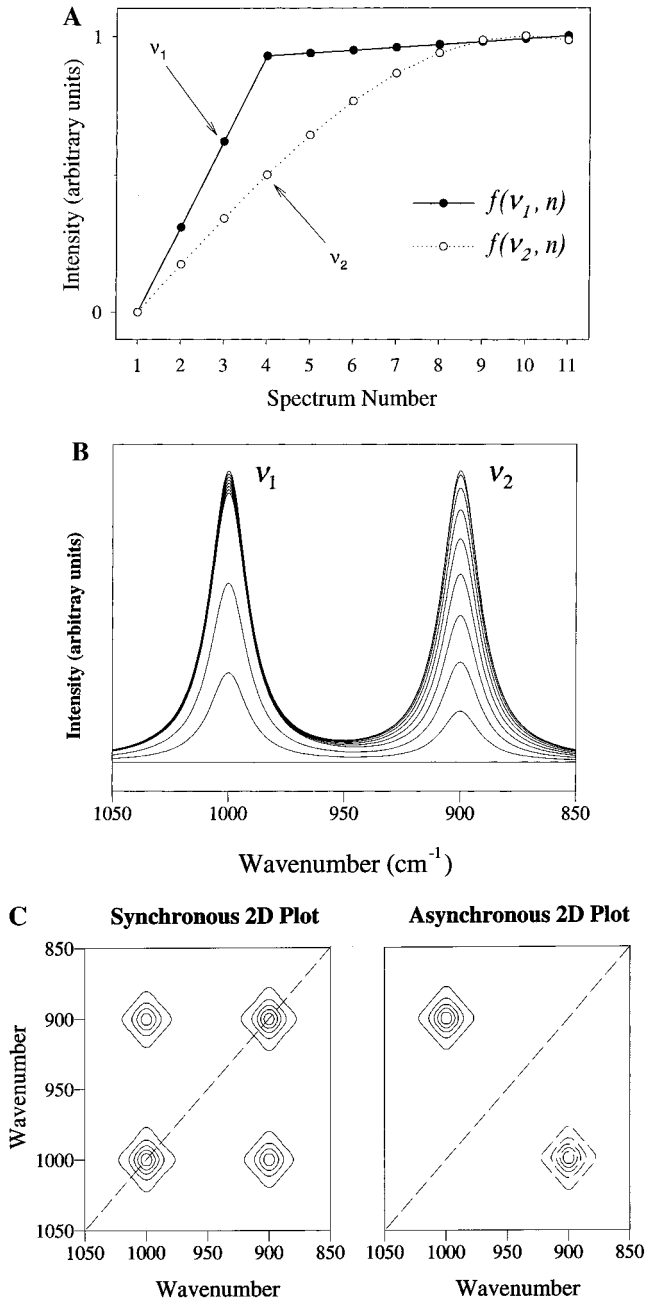

Figure 1. Qualitative use of 2D IR to determine sequential spectral events using Noda's rules, as described in the text. The band intensities at two independent wavenumbers ν_1 and ν_2 vary independently with different functional forms through a data set of 11 sequentially collected spectra. **(A)** Plot of how the band intensities at ν_1 and ν_2 change through the data set. For ν_1 the band intensities change as a two-step linear function, whereas ν_2 the band intensities change as a partial sine function. **(B)** Simulated spectra illustrating how the band intensities at ν_1 and ν_2 change for the 11 spectra. Peaks at ν_1 (1000 cm^{-1}) and ν_2 (900 cm^{-1}) were calculated as Lorentzian bands with fwhm of 20 cm^{-1} and a resolution of 1 cm^{-1}. The band intensities for ν_1 and ν_2 vary through the 11 spectra according to the mathematical relationships shown in Figure 1A. **(C)** Synchronous and asynchronous 2D IR correlation plots calculated from the simulated spectra shown in Figure 1B. Positive correlation intensities are indicated by a solid line; negative correlation intensities are indicated by a dashed line.

the event at ν_1 occurs before the event at ν_2. That is, the event at $f(\nu_1,n)$ leads and $f(\nu_2,n)$ lags, which confirms our intuitive prediction.

II. $\beta\nu$ Correlation Analysis: A Modified 2D IR Method for Determining Temporal Relationships. As described above, a standard generalized 2D IR algorithm can be used to qualitatively describe the degree of coherence (i.e., the synchronous plot) or incoherence (i.e., the asynchronous plot) between the intensity variations of two signals in a set of dynamic spectra. In appropriate situations, the algorithm can also be used to qualitatively determine the temporal sequence of spectral events.

In this section, we present a modified 2D IR method that can more quantitatively describe the degree of coherence between spectral intensity variations in a discrete set of dynamic spectra. This is possible if we assume that the measured spectral band intensities at, for example, ν_1 and ν_2, vary with some defined mathematical form. For example, consider the spectral intensity variation $f(\nu,n)$ and a discrete sinusoidal function $f(\beta,n) = \sin(k\phi + \beta)$ that approximates how the IR band intensity at frequency ν varies in a set of n spectra. For these two functions, an asynchronous cross correlation of $f(\nu,n)$ with $f(\beta,n)$ can be performed where β is varied. We call this type of cross correlation a *$\beta\nu$ correlation*. The maximum positive correlation intensity will be observed at one point (ν, β) in the asynchronous 2D plot for the range $360° > \beta \geq 0°$. This point is used to define a new parameter − the effective phase angle β_e of $f(\nu,n)$. The value β_e is simply equal to $\beta + 90°$. Like a true phase angle, the β_e values can be used to establish the sequence of spectral events in a set of dynamic spectra. It will be shown in the next section that spectral events with larger β_e values occur before spectral events with smaller β_e values when the signal intensities vary according to a defined model.

$\beta\nu$-Correlation Analysis. A $\beta\nu$ correlation analysis is a mathematical asynchronous cross correlation performed on a set of dynamically varying IR spectra against a set of sinusoidal functions which differ only by their phase angle β. This correlation analysis is mathematically described using eq 5

$$\Psi(\nu,\beta) = \frac{1}{N-1}\sum_{j=0}^{N-1} f(\nu,n_j)\cdot\sum_{k=0}^{N-1} M_{jk}\cdot\sin(k\phi+\beta) \qquad (5)$$

The correlation intensity Ψ at some point (ν,β) represents the correlation of the measured IR spectral intensity $f(\nu,n_j)$ with the mathematical function $\sin(k\phi + \beta)$. In eq 5, f is the IR intensity, ν is the frequency or wavenumber, n_j is the number of the spectrum in the ordered sequence where the first spectrum number is zero, β is the phase angle of the respective sine function, N represents the total number of spectra used in the calculation, ϕ is a constant value in degrees (or radians) chosen based upon the total number of dynamic spectra used in the calculation, and M_{jk} is the Hilbert transform matrix, which was previously defined in eq 4. In this manuscript, all $\beta\nu$ correlations were performed with $\phi = 10°$ so that $\sin(k10° + \beta)$ describes approximately $^1/_4$ of the cycle of a sine function, or the approximate form of a commonly observed variation in spectral band intensities upon sample perturbation.

Only the asynchronous correlation algorithm is used in the $\beta\nu$ correlation analysis presented here. Although it is also possible to perform this analysis using the synchronous algorithm, we have confined our discussion to the use of the asynchronous correlation because it is more sensitive to differences in the form of signal variations than the synchronous correlation.[1]

The effective phase angle, β_e, is defined by eq 6

$$\beta_e = \beta + 90° \qquad (6)$$

In eq 6, β is the point of maximum positive correlation intensity in the plot of β *versus* ν defined by eq 5. The value of β_e is defined

in this fashion so that the phase angle β and the effective phase angle β_e are the same for a sinusoidal signal variation with constant frequency. In this paper, we refer to β_e *vs* ν asynchronous correlation maps as $\beta\nu$ plots.

It should be noted at this point that one can determine an unknown phase angle (e.g., β_1) for a sinusoidal signal variation, for example, sin $(\Theta + \beta_1)$, using a sinusoidal test function, such as sin $(\Theta + \beta_2)$, where β_2 is known and can be varied. When sin $(\Theta + \beta_1)$ and sin $(\Theta + \beta_2)$ are cross correlated, the maximum correlation intensity is observed in the conventional synchronous 2D IR plot when $\beta_2 = \beta_1$, and the maximum correlation intensity is observed in the conventional asynchronous 2D IR plot when $\beta_2 = \beta_1 + 90^0$.

Example of a $\beta\nu$ Plot. To illustrate the kind of information that is available in a $\beta\nu$ plot, a $\beta\nu$ correlation analysis was performed on three discrete sets of simulated spectra. The respective $\beta\nu$ plots for these spectra are presented in Figure 2. For the spectra used in the $\beta\nu$ correlation analysis shown in Figure 2, all three sets of simulated spectra contained two well-resolved peaks at $\nu_1 = 1000$ cm^{-1} and $\nu_2 = 900$ cm^{-1}; these bands were created with Lorentzian band shapes having a fwhm of 20 cm^{-1} and a resolution of 1 cm^{-1}.

In Figure 2A, the $\beta\nu$ correlation plot is presented for the first set of simulated spectra. In this case, the two peaks at two independent wavenumbers ν_1 and ν_2 vary in an identical and in-phase sinusoidal manner through a data set of 21 sequentially collected spectra; therefore, the phase angle difference β for ν_2 relative to ν_1 is equal to 0°. The conventional 2D IR correlation maps in conjunction with Noda's rules would indicate that both events occur simultaneously. This can be quantitatively observed from the $\beta\nu$ correlation plot (Figure 2A). In this figure $\beta e = 0$ for ν_1 at 1000 cm^{-1} and $\beta e = 0$ for ν_2 at 900 cm^{-1}; therefore the β_e effective phase angle values faithfully reproduce the actual phase angle value and indicate that both events occur simultaneously.

A similar analysis is presented in Figure 2B for the second set of simulated spectra. In this case, two peaks at two independent wavenumbers ν_1 and ν_2 also vary in an identical sinusoidal manner through a data set of 21 sequentially collected spectra as do the bands in the first set of simulated spectra (Figure 2A). In this case, however, the spectra vary out-of-phase relative to one another. In this out-of-phase sinusoidal relationship, the phase angle β for theν_2 band at 900 cm^{-1} is advanced by 45° relative to theν_1 band at 1000 cm^{-1}. A conventional 2D IR correlation analysis in conjunction with Noda's rules would indicate that the ν_2 band at 900 cm^{-1} will occur before the ν_1 band at 1000 cm^{-1} because the phase angle β for ν_2 is advanced relative to ν_1. The $\beta\nu$ correlation plot for this case easily demonstrates this principle (Figure 2B). In this figure $\beta e = 0$ for ν_1 at 1000 cm^{-1} and $\beta e = 45$ for ν_2 at 900 cm^{-1}. Therefore, the βe effective phase angle values again reproduce the actual phase angle values and indicate that the event at ν_2 occurs before the event at ν_1.

Finally, Figure 2C presents the $\beta\nu$ correlation analysis for the third set simulated spectra, which are presented in Figure 1. In this case, the band intensities for two peaks at two independent wavenumbers ν_1 and ν_2 vary in completely different functional forms, namely a two-step linear function and a partial sine wave. The temporal analysis of these band intensities on the basis of standard 2D IR methods is somewhat more complicated, but would demonstrate that ν_1 should occur before ν_2. From the $\beta\nu$ plot in Figure 2C we see that the effective phase angle of $f(\nu_2, n)$, the partial sine wave, is $\beta_e = 0.5°$, and the effective phase angle of $f(\nu_1, n)$, the two-step linear function,

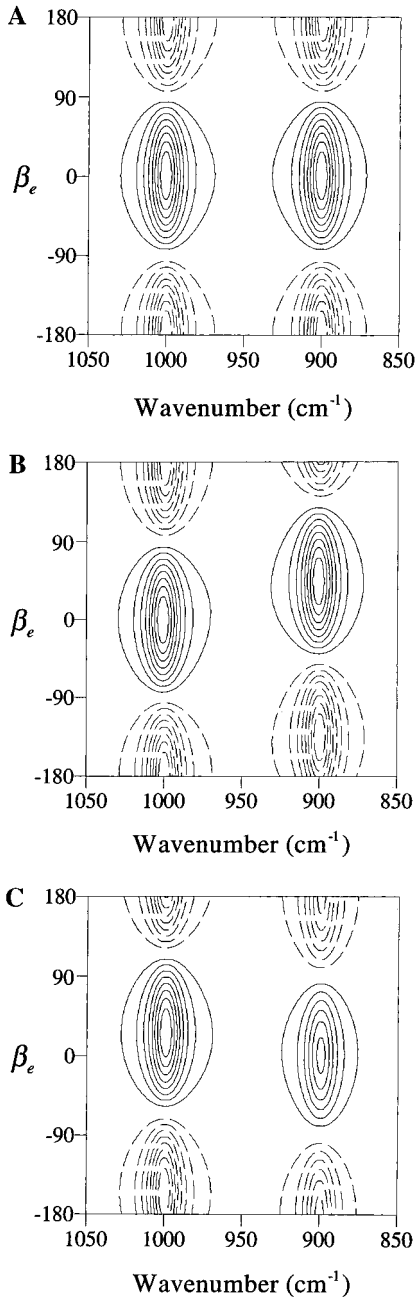

Figure 2. Examples of $\beta\nu$ correlation plots for different sets of simulated spectra as described in the text. For all plots, positive correlation intensities are indicated by a solid line; negative correlation intensities are indicated by a dashed line. **(A)** $\beta\nu$ correlation plot for the case in which two peaks at two independent wavenumbers ν_1 and ν_2 vary in an identical and in-phase sinusoidal manner through a data set of 21 sequentially collected spectra. Since $\beta e = 0$ for ν_1 at 1000 cm^{-1} and $\beta e = 0$ for ν_2 at 900 cm^{-1}, both events occur simultaneously. **(B)** $\beta\nu$ correlation plot for the case in which two peaks at two independent wavenumbers ν_1 and ν_2 vary in an identical but out-of-phase sinusoidal manner through a data set of 21 sequentially collected spectra. Since $\beta e = 0$ for ν_1 at 1000 cm^{-1} and $\beta e = 45$ for ν_2 at 900 cm^{-1}, the event at ν_2 occurs before the event at ν_1. **(C)** $\beta\nu$ correlation plot for the case in which two peaks at two independent wavenumbers ν_1 and ν_2 vary in completely different manners through a data set of 11 sequentially collected spectra. Because $\beta e = 25.5$ for ν_1 at 1000 cm^{-1} and $\beta e = 0.5$ for ν_2 at 900 cm^{-1}, the event at ν_1 occurs before the event at ν_2.

is $\beta_e = 25.5°$. On the basis of these values, we can say that the event at ν_1 occurs before the event at ν_2 because $\beta_e = 25.5° > \beta_e = 0.5°$. The conclusion is the same as that obtained using standard 2D IR spectra and Noda's rules; however, using the

$\beta\nu$ plot we can quantify the difference in the effective phase angle, i.e., $\Delta\beta_e = 25.0°$. Because $\Delta\beta_e$ is reasonably large, we know that our assumption can be made with a large degree of confidence. A discussion of the level of uncertainty inherent in the calculation of β_e is presented in the next section.

On the basis of the above discussion it is apparent that a $\beta\nu$ correlation analysis plot provides a number of desirable features, including: (1) the degree of coherence between signal variations and the sequence of spectral events, i.e., the relative rates of signal variation, are immediately revealed in the $\beta\nu$ plot; (2) $\beta\nu$ correlation plots are relatively easy to calculate in that they require no Fourier transformations; (3) β_e is a direct result of the correlation analysis, i.e., no additional calculations are required; (4) in appropriate situations β_e values from different experiments may be compared; and (5) although the amount of noise observed in any 2D correlation plot is ultimately determined by the amount of noise in the spectra used in the correlation, noise is observed at a lower level in a $\beta\nu$ correlation plot than the standard 2D IR maps.

The issue of noise in a $\beta\nu$ correlation plot is easily appreciated by examining eqs 3 and 7. In a standard 2D IR correlation analysis, a measured signal variation with noise (or uncertainty) is correlated against another measured signal variation with noise. However, in a $\beta\nu$ correlation analysis a measured signal variation with noise is correlated against a mathematical function with no noise. The effect of this situation on correlation intensities can be summarized mathematically as [(true value + uncertainty) × (true value)] in a $\beta\nu$ plot compared to [(true value + uncertainty) × (true value + uncertainty)] in a conventional 2D IR plot.

The effect of noise can be significant when an average spectrum is used as the reference spectrum for calculating the series of dynamic spectra, as is a common procedure in the 2D IR method. In the usual case, an average spectrum is subtracted from each spectrum in the set and the resulting set of difference spectra, i.e., the dynamic spectra, are cross-correlated. Therefore, the effect of noise in the 2D plots is more pronounced when small relative signal variations are observed in the set of dynamic spectra as compared to large signal variations. This effect has previously been described in detail.[29] A recent article[27] has also considered the effects of noise in 2D correlation maps using the ratio of asynchronous to synchronous correlation functions and is particularly relevant to $\beta\nu$ correlation analysis.

III. A Simple Rate Model for Describing Intensity Variations and Their Effect on β_e. As mentioned earlier, β_e can be used to quantitatively determine the temporal relationships and the degree of coherence between IR intensity variations in any discrete set of dynamic spectra. Additionally, β_e allows correlations from separate experiments to be compared. To accomplish this, however, the form of the IR intensity variation in the measured dynamic spectral data set must be described and approximated by a mathematical model.

In this section, we explore how a specific mathematical form of intensity variation can affect the corresponding β_e value. We describe a model for relative rates that includes several different possible paths of intensity variation for an absorption band in a set of dynamic spectra. The model can then be used to explore how the β_e value responds to changes in band intensity. In doing so, the model can establish a relationship between β_e and the relative rates of intensity change for a set of time-resolved absorption bands. The model also can be used to investigate the level of uncertainty expected in the β_e values calculated from experimental data.

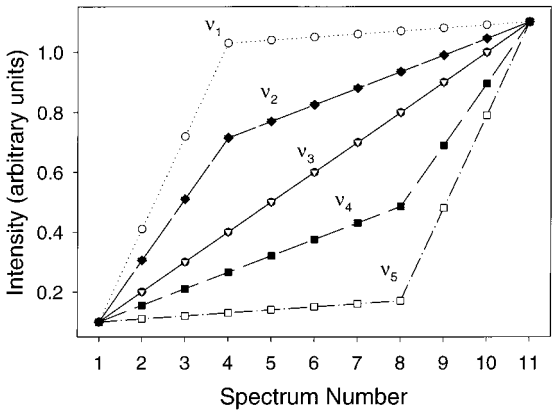

Figure 3. Variation of band intensity for five independent peaks that describe the 'intensity change' model. Plot of how the band intensities at ν_1,ν_2,ν_3,ν_4, and ν_5 change through a data set of 11 sequentially collected spectra.

In general, the model exploits the same phase angle relationship between two varying signals as previously described.[1] However, by simulating time-resolved absorption bands according to the various intensity variations described by the model, inherent uncertainities may be addressed in a practical manner. These uncertainities are caused by such things as overlapping peaks, frequency shifts, changes in bandwidths and the appearance of bands with both increasing and decreasing intensities. Most importantly, a β_e − relative rates model allows a researcher to establish what value contitutes a significant difference in β_e for two different spectral frequencies in the dynamic spectra.

Consider a set of time-resolved IR spectra that are collected as a sample undergoes some type of sample perturbation, such as a stress−strain cycle or thermodynamic phase transition. In Figure 3, a model is presented that uses five possible paths to illustrate the form that a change in IR intensity can potentially assume as the sample changes during the perturbation. These paths of intensity change were chosen since they are commonly observed during the beginning half of a thermodynamic phase transition, a specific example of which is considered in Section IV. We shall refer to this model as the 'intensity change' model.

It is apparent from Figure 3 that the spectral intensity change at ν_1 begins before the intensity change at ν_2, that is to say the initial relative rate of change at ν_1 is greater than the initial rate of change at ν_2. The entire sequence of spectral events in Figure 3 can be summarized as $\nu_1 \rightarrow \nu_2 \rightarrow \nu_3 \rightarrow \nu_4 \rightarrow \nu_5$, where the symbol "→" means "occurs before".

Two sets of simulated time-resolved spectra were generated for the 'intensity change' model using the five possible paths shown in Figure 3. These simulated spectra are presented in Figure 4A and 4B. In the first set shown in Figure 4A, five absorption bands are well resolved and are located at 1000, 980, 960, 940, and 920 cm^{-1}. These five peaks are identified as bands ν_1, ν_2, ν_3, ν_4, and ν_5. These well-resolved peaks were simulated with Lorentzian band shapes having a fwhm of 5 cm^{-1} and a resolution of 1 cm^{-1}. In the second set of spectra shown in Figure 4B, the five overlapped peaks are calculated using the same parameters as the spectra in Figure 4A, with the exception that the fwhm of the Lorentzian band shapes was 20 cm^{-1} for each of the five peaks.

In Figures 4A and 4B, the band intensities for each of the five peaks increase at independent rates as the data set progresses, according to the specific mathematical relationship for bands ν_1, ν_2, ν_3, ν_4, and ν_5 described in the 'intensity change' model shown in Figure 3. A $\beta\nu$ correlation analysis was

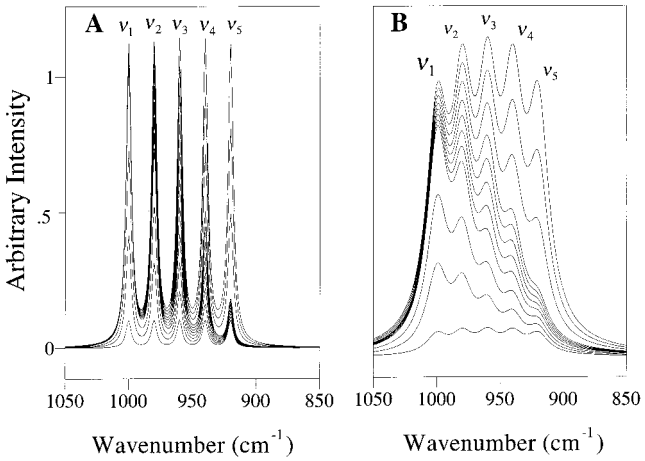

Figure 4. Simulated spectra illustrating how the band intensities at ν_1,ν_2,ν_3,ν_4, and ν_5 change for the 11 spectra according to the 'intensity change' model. Peaks were calculated as Lorentzian bands at a resolution of 1 cm^{-1} for ν_1 (1000 cm^{-1}), ν_2 (980 cm^{-1}), ν_3 (960 cm^{-1}) ν_4 (940 cm^{-1}) and ν_5 (920 cm^{-1}). The band intensities for ν_1 through ν_5 vary through the 11 spectra according to the mathematical relationships shown in Figure 5. **(A)** 'Intensity change' model with well-resolved peaks. All peaks were calculated using a fwhm of 5 cm^{-1}. **(B)** 'Intensity change' model with overlapping peaks. All peaks were calculated using a fwhm of 20 cm^{-1}.

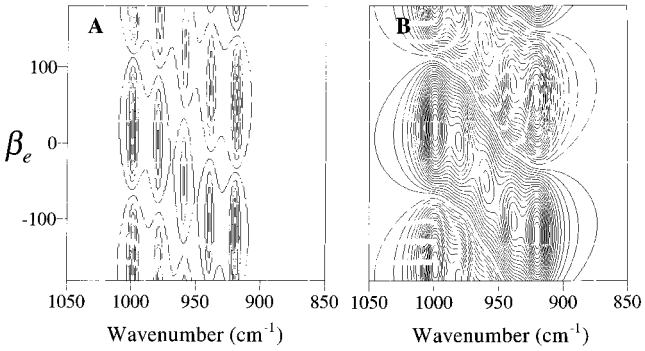

Figure 5. The $\beta\nu$ correlation plots for the simulated spectra illustrated in Figure 4. For both Figure 5A and 5B, positive correlation intensities are indicated by a solid line; negative correlation intensities are indicated by a dashed line. Specific β_e values obtained from these plots are tabulated in Table 1. **(A)** $\beta\nu$ correlation plot for the 'intensity change' model with well-resolved peaks of Figure 4A. **(B)** $\beta\nu$ correlation plot for the 'intensity change' model with overlapping peaks of Figure 4B.

performed using the time-resolved spectra presented in Figure 4A, which features well-resolved bands. The $\beta\nu$ plot that resulted from this calculation is presented in Figure 5A, while the corresponding β_e values for the well-resolved peaks were obtained from this $\beta\nu$ plot and are presented in Table 1. The β_e values tabulated in Table 1 for these well-resolved spectra are spread over a range that is 150.0° wide and correctly determine the relative rates of intensity change in the five peaks in this model. That is, the β_e values 25.0° > 4.9° > −50.1° > −104.5° > −125.0° indicate that $\nu_1 \rightarrow \nu_2 \rightarrow \nu_3 \rightarrow \nu_4 \rightarrow \nu_5$, just as is defined in the 'intensity change' model in Figure 5. These data clearly demonstrate that β_e values can be used to establish the relative rates of change in the band intensities of a set of time-resolved spectra whose intensity changes are modeled by a defined mathematical function.

A $\beta\nu$ correlation analysis was also performed using the time-resolved spectra presented in Figure 4B, which features heavily overlapped bands. The corresponding $\beta\nu$ plot is presented in Figure 5B, and the corresponding β_e values from the overlapped bands of Figure 5B are also presented in Table 1. The β_e values

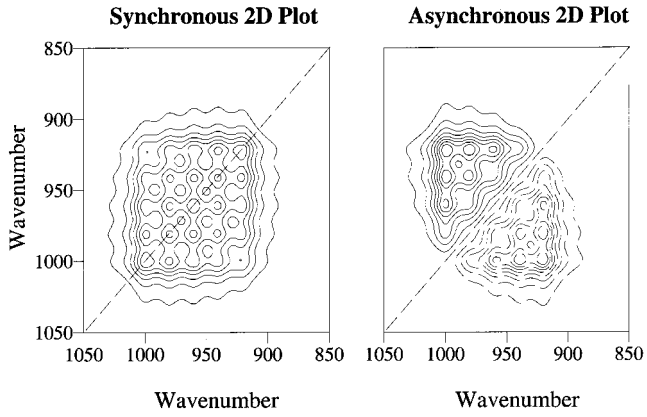

Figure 6. Standard 2D IR synchronous and asynchronous correlation plots for the 'intensity change' model with overlapping bands. These 2D correlation plots were calculated from the simulated spectra of the 'intensity change' model with overlapping peaks shown in Figure 4B.

TABLE 1: Values for the Effective Phase Angle, βe, Obtained from the $\beta\nu$ Correlation Plots of the 'Intensity Change' Model in Figure 5. Symbols: WR = well-resolved, OV = overlapped

peak wavenumber position, cm^{-1}	βe values well-resolved peaks model	βe values overlapped peaks model	$\Delta\beta e$ values βe (WR) − βe (OV)
1000	25.0	21.0	−4.0
980	4.9	2.5	−2.4
960	−50.1	−50.0	0.1
940	−104.5	−102.3	2.2
920	−125.0	−120.9	4.1

for this case are spread over a range that is 141.9° wide and also correctly predict the relative rates of intensity change in the five overlapped peaks. That is, the β_e values 21.0° > 2.5° > −50.0° > −102.3° > −120.9° indicate that $\nu_1 \rightarrow \nu_2 \rightarrow \nu_3 \rightarrow \nu_4 \rightarrow \nu_5$. Although the original bands from which the $\beta\nu$ plot was calculated are highly overlapped (see Figure 4B), reliable β_e values were obtained for all five of these overlapping bands.

A comparison of the β_e values listed in Table 1 for each peak in the two limiting cases (i.e., well-resolved or overlapping) demonstrates that bandwidth, at least, is not a factor that prohibits determination of reliable β_e values for broad, overlapped bands. In fact, Table 1 shows that each of these peaks can be calculated with an absolute error of less than or equal to 4.1° (calculated as |overlapped β_e − resolved β_e|). Clearly, β_e values can also be used to establish the temporal relationship of overlapping IR bands in an experimental set of time-resolved spectra, which are well approximated by the 'intensity change' model. A more thorough description of how various band parameters, e.g., frequency shifts, bandwidth and mathematical functions, affect β_e values is beyond the scope of this paper and will be presented elsewhere.

For the sake of comparison with the $\beta\nu$ method, the standard 2D IR synchronous and asynchronous correlation plots were also calculated for the 'intensity change' model with overlapping peaks using the spectra in Figure 4B. These correlation maps are presented in Figure 6. Although the temporal relationships among the five bands can be determined using the synchronous and asynchronous 2D plots presented in Figure 6, visualizing these relationships requires a more elaborate procedure using the signs of the cross-peaks and Noda's rules to establish the relative rates. In contrast, the temporal relationships among the ν_1 through ν_5 bands are immediately revealed in the $\beta\nu$ − plot from the β_e values (compare Figure 6 with Figure 5B).

Furthermore, because β_e has a numerical value, it can be used to quantitatively investigate the uncertainty in the determination.

The 'intensity change' model illustrated in Figures 3−5 describes a situation in which the IR band intensities $f(\nu,n)$ all increase with time; however, IR band intensities can also decrease when samples undergo an external perturbation. It is possible to show that the β_e parameter exhibits the same behavior for decreasing IR intensities as it does for increasing intensities. In fact, the same model described above becomes applicable to the situation where the IR intensities decrease with time simply by multiplying IR band intensities $f(\nu,n)$ by negative one, i.e., $-f(\nu,n)$. In the case of decreasing IR intensities, spectral bands with larger β_e values will also occur before spectral events with smaller β_e values. Because the model for the decreasing intensities is essentially the same as the one for increasing intensities, we have chosen not to duplicate the analysis.

These two limiting cases, i.e., all band intensities increasing or all band intensities decreasing are the easiest to describe. However, the intermediate case in which some IR bands increase in intensity while others decrease in intensity through the data set is more complicated. In this case, the β_e values calculated for the increasing and decreasing bands are not comparable on the same scale. One way to obtain directly comparable β_e values for simultaneously increasing and decreasing band intensities is to "transform" the decreasing signals into increasing signals by multiplying the decreasing signal variations by negative one. The resulting β_e values will then be directly comparable and can be used to establish the relative rates of change for bands that both increase and decrease in a data set.

This transformation process is cumbersome; fortunately, it is also not necessary. Using eq 5 in combination with the trigonometric identity $-\sin(\theta) = \sin(\theta \pm 180°)$ it can be shown that the β_e value for an increasing band intensity (i.e., $f(\nu,n)$) simply differs from the β_e value for a decreasing band intensity (i.e., $-f(\nu,n)$) by $\pm 180°$. Therefore, directly comparable β_e values are obtained by simply adding or subtracting 180° to or from the β_e values for the decreasing signal intensities (i.e., $-f(\nu,n)$) and leaving the β_e values for the increasing signal intensities (i.e., $f(\nu,n)$) uncorrected.

It is relative easy to show that adding or subtracting 180° to or from the β_e values from decreasing band intensities makes these values directly comparable to the β_e values calculated from increasing band intensities. When a $\beta\nu$ correlation analysis is performed on a decreasing band intensity, (i.e., $-f(\nu,n)$), the maximum positive correlation intensity, Ψ, is observed at one point, (ν,β_1) in the $\beta\nu$ correlation plot for the range $360° > \beta_1 \geq 0°$. The value of $\Psi(\nu,\beta_1)$ for a decreasing band intensity is defined in eq 7

$$\Psi(\nu,\beta_1) = \frac{1}{N-1}\sum_{j=0}^{N-1} -f(\nu,n_j)\cdot\sum_{k=0}^{N-1} M_{jk}\cdot\sin(k\phi+\beta_1) \quad (7)$$

Note that eq 7 for decreasing intensities is directly analogous to eq 5 for increasing band intensities with the exception of the negative sign. Also, as described above, the point (ν,β_1) can be used to define the effective phase angle β_e of $-f(\nu,n)$, i.e., $\beta_e = \beta_1 + 90°$.

If $f(\nu,n_j)$ is substituted for $-f(\nu,n_j)$ in eq 7, $-\sin(k\phi+\beta_1)$ must also be substituted for $\sin(k\phi+\beta_1)$ in order to leave $\Psi(\nu,\beta_1)$ unaltered. This is demonstrated in eq 8

$$\Psi(\nu,\beta_1) = \frac{1}{N-1}\sum_{j=0}^{N-1} f(\nu,n_j)\cdot\sum_{k=0}^{N-1} M_{jk}\cdot -\sin(k\phi+\beta_1) \quad (8)$$

A simple substitution using trigonometric identities allows us to describe the relationship between the increasing and decreasing β_e values without a full calculation. Because $-\sin(\theta) = \sin(\theta \pm 180°)$, then

$$-\sin(k\phi+\beta_1) = \sin(k\phi+\beta_1 \pm 180°) \quad (9)$$

If we define $\beta_2 = \beta_1 \pm 180^0$, then

$$-\sin(k\phi+\beta_1) = \sin(k\phi+\beta_2) \quad (10)$$

In this case, $\beta_{e2} = \beta_2 + 90^0$, where β_{e2} is the effective phase angle for the decreasing intensity bands that is needed for direct comparison with β_e, the value calculated for the increasing bands. The β_e and β_{e2} values can be related as follows

$$\beta_{e2} = \beta_2 + 90^0$$

$$\beta_{e2} = (\beta_1 \pm 180°) + 90^0$$

$$\beta_{e2} = (\beta_1 + 90°) \pm 180^0$$

$$\beta_{e2} = \beta_e \pm 180^0 \quad (11)$$

IV. Application of $\beta\nu$ Correlation Analysis to the Solid−Solid-Phase Transition of *n*-Nonadecane. The following application illustrates the ability of $\beta\nu$ correlation analysis for determining relative rates of intensity change. In this case, the relative rates of change in the submolecular groups of a hydrocarbon during a thermodynamic phase transition are observed by IR spectroscopy. It is well-known that *n*-nonadecane (*n*-$C_{19}H_{40}$) undergoes a solid−solid-phase transition from an orthorhombic phase I to a hexagonal phase II at ∼22.5 °C.[30−32] This is the so-called "rotator" transition. In previous studies, conformationally sensitive methylene wagging (CH_2 W) modes have been used to locate and quantify the number of gauche defects along the polymethylene chain just before and after the phase transtion.[33,34] However, to our knowledge, no IR study has been performed in which time-resolved spectra were collected continuously as the alkane passed through this phase I−phase II transition at constant temperature. In this application, we use $\beta\nu$ correlation analysis to study the relative rates of conformational change for three different types of gauche defects and for the orthorhombic-to-hexagonal unit cell for *n*-$C_{19}H_{40}$. We then show how these results can be used to propose a possible mechanism for the phase transition.

Time-resolved IR spectra were continuously collected as the alkane slowly passed through the phase I to phase II transition. To accomplish this, a spectrum was acquired every five seconds while the temperature of the sample cell was raised from below room temperature to 22.5 °C, and then held at ∼0.5 °C above the transition temperature. A set of 11 IR spectra was chosen for the $\beta\nu$ correlation analysis. This set of spectra represents the first half of the orthorhombic (phase I) − hexagonal (phase II) transition.

The spectra of *n*-nonadecane obtained during the phase transition are presented in Figure 7. The bands of interest in this study are highlighted in this spectrum. These bands include the weak, conformationally sensitive, CH_2 W modes at ∼1368 cm^{-1} ("kink"- GTG*), 1352 cm^{-1} ("double gauche" − GG), 1342 cm^{-1} ("end gauche" − TG), and 766 cm^{-1} ("end gauche" − TG).[31,33−36] Also of interest are the methylene rocking (CH_2 P) modes near 745 cm^{-1}. Factor-group splitting is observed for orthorhombic unit cells (phase I); whereas no factor-group splitting is observed for hexagonal unit cells (phase II).[37] In

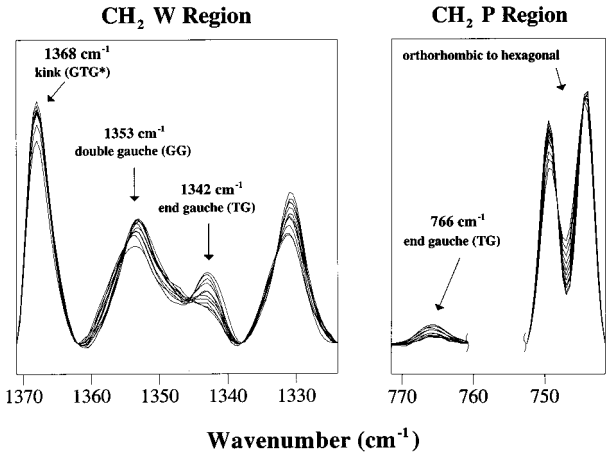

Figure 7. Time-resolved IR spectra of *n*-nonadecane used in the correlation analysis correspond to the first half of the solid−solid-phase transition for *n*-nonadecane**. (A)** Methylene wagging region of interest **(B)** methylene rocking region of interest.

this set of spectra, the CH_2 P bands near 730 cm^{-1} had absorbance values greater than one and therefore were not used.

Unfortunately, the IR spectra for *n*-$C_{19}H_{40}$ are complicated by partially overlapping strong and weak bands. Furthermore, in general, IR absorbances decrease as the alkane passes through the phase transition. To reduce the effect of these problems, spectra were normalized against the symmetric methyl deformation ("umbrella") band (CH_3 U) near 1378 cm^{-1}. This band is insensitive to changes in conformation and is therefore suitable for use as an intensity reference standard. The frequency and fwhm of the CH_3 U band were measured, and a pure Lorentzian band with this frequency and fwhm was subtracted from the spectrum.

The set of time-resolved IR spectra produced after these normalizations and used in the $\beta\nu$ correlation analysis are presented in Figure 7. In the spectra presented in Figure 7, a multicomponent baseline correction was performed in the ranges 1371−1338 cm^{-1} and 772−741 cm^{-1}. The baseline correction was performed not only for display purposes but also to prepare the spectra for input into the calculation of the asynchronous $\beta\nu$ plots.

The asynchronous $\beta\nu$ correlation plots associated with the spectra in Figure 7 are presented in Figure 8. The effective phase angles, β_e, obtained from Figure 8 are presented in Table 2. Notice from Table 2 that some of the β_e values are positive, whereas others are negative. The negative β_e values correspond to bands whose intensities increase as the sample passes through the phase transition, whereas the positive β_e values correspond to bands whose intensities decrease as the sample passes through the phase transition. This can be confirmed from inspection of the time-resolved spectra. To obtain directly comparable β_e values for both the increasing and the decreasing band intensities, 180° was added to the β_e values calculated for the increasing band intensities. The justification for this approach was described in the previous section.

Using the time-resolved IR spectra shown in Figure 7 and the $\beta\nu$ plot presented in Figure 8, we can monitor the following events: (1) the change in number of "end gauche" or TG conformers from the bands at 1342 and 766 cm^{-1}; (2) the change from orthorhombic to hexagonal unit cell from the band at 750 and 745 cm^{-1}; (3) the change in number of "double gauche" or GG conformers from the band at 1353 cm^{-1}; and (4) the change in the number of "kink" or GTG* conformers from the band at 1368 cm^{-1}.

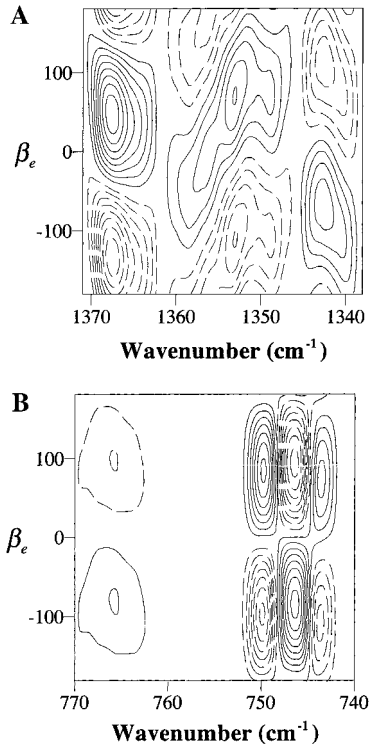

Figure 8. $\beta\nu$ correlation plot for the first half of the solid−solid-phase transition for *n*-nonadecane. **(A)** Methylene wagging modes−region of interest. **(B)** Methylene rocking modes−region of interest.

TABLE 2: Values for the Effective Phase Angle, βe, Obtained from the $\beta\nu$ Correlation Plots (Figure 7) for the Phase Transition of *n*-Nonadecane as it Undergoes its Phase I − Phase II (Orthorhombic−Hexagonal) Phase Transition

peak wavenumber position, cm^{-1}	assignment	initial βe values	adjustment	comparable βe values
1368	kink	46		46
1353	double gauche	73		73
1342	end gauche	−71	+180	109
766	end gauche	−76	+180	104
750	orthorhombic	84		84
745	hexagonal	−86	+180	94

The intensities observed at 1368 and 1353 cm^{-1} in the time-resolved spectra (Figure 7), suggest the existence of a very small number of "kink" and "double gauche" defects in phase I at the beginning of the phase transition. From the effective phase angles listed in Table 2, the following observations can be made from the $\beta\nu$ plot.

(1) The two bands that correspond to the orthorhombic and hexagonal packing arrangements at 750 and 745 cm^{-1} are nearly anti-phase. This relationship is expected since the orthorhombic band at 750 cm^{-1} should be decreasing at the same rate at which the hexagonal band at 745 cm^{-1} increases. Note that the phase angle difference between the β_e values of these two bands (84° vs −86°) is nearly 180° (anti-phase).

(2) The bands located at 1342 and 766 cm^{-1} have similar β_e values. This also is expected since both vibrational modes are assigned to "end gauche" conformers.

(3) The following relative rates of change in signal variation are assigned using the β_e values in Table 2: 1342 cm^{-1} (increasing TG) ≈ 766 cm^{-1} (increasing TG) → 750 cm^{-1} (decreasing orthorhombic structure) ≈ 745 cm^{-1} (increasing hexagonal structure) → 1353 cm^{-1} (decreasing GG) → 1368 cm^{-1} (decreasing GTG*), where "→" means "occurs at a faster

rate" or "occurs before" and $\approx$ means "occurs at the same rate" or "occurs at the same time".

These data show that the "end gauche" defects are created at a faster relative rate than the hexagonal unit cells. The hexagonal unit cells are created at a faster rate than the number of "double gauche" defects decrease. In addtion, hexagonal unit cells are created faster than the number of "kink" defects decreases. Finally, the number of "double gauche" defects decreases at a faster relative rate than the number of "kink" defects.

The effective phase angle values tabulated in Table 2 allow us to propose a possible mechanism for the rotator phase transtion in *n*-nonadecane.

Step 1: The pre-transition state is a mixture of a very large amount "all trans" conformers with a very small fraction of the chains containing "kinks" with "double gauche" conformer defects in a orthorhombic lamellar structure

Step 2: The lamellar structure is disrupted by the protrusion of a number of "all trans" conformers form the lamellae, with the concurrent formation of "end gauche" defects in these chains.

Step 3: A smaller number of "kink" with "double gauche" conformers change to a "kink" with "end gauche" conformer.

Step 4: These "kink" with "end gauche" conformers subsequently change to an "all trans" with "end gauche" conformer.

The "kink" and "end gauche" defects reappear in much larger concentrations as the temperature increases in phase II, however, the mechanism described here only refers to the pure phase transition between phase I and phase II, and not any temperature dependent changes that may occur as the temperature increases in phase II. The findings are generally in agreement with those originally reported by Zerbi et al.[31,38] with the exception that Zerbi's model describes the pretransition state of the alkane as simply "all trans". Our model includes a small number of "kink" and "double gauche" conformer defects that exist and participate in the phase transition. These results demonstrate the power of $\beta\nu$ correlation analysis for determining relative rates of intensity change in vibrational spectroscopy.

V. A Comparison of $\beta\nu$ Correlation Analysis With Conventional 2D IR. In addition to the $\beta\nu$ correlation plots shown in Figure 8, we have also calculated the synchronous and asynchronous 2D IR correlation maps and performed a conventional 2D IR correlation analysis on the time-resolved IR spectra of nonadecane undergoing its phase I $-$ phase II transition, shown in Figure 7. Inspection of these calculated 2D IR plots (data not shown) confirms that the application of standard 2D IR theory in conjunction with the signs of the cross-peaks can also indicate relative rates of change in these spectra, albeit more qualitatively and with more subjective interpretation.

Like conventional 2D IR methods, $\beta\nu$ correlation analysis can provide enhanced resolution in the asynchronous 2D plots. This is especially apparent in the $\beta\nu$ correlation plots presented in Figure 8B in which the orthorhombic singlet and doublet are clearly resolved. These bands are heavily overlapped in the time-resolved IR spectra presented in Figure 7B. However, unlike conventional 2D IR, the extent to which resolution is enhanced is limited by the mathematical function used in the $\beta\nu$ correlation. In other words, the ability to produce β_e values in a wide range depends on the specific mathematical function used and its apparent suitability to the process under study. In the present case, we have only considered a sine function of $^1/_4$ cycle to approximate the intensity variation through the spectral data set. However, we have also performed preliminary correlation analyses with exponential, Gaussian and two-step linear functions to gain more practical insight into which mathematical forms might best model specific intensity variations. Such work is beyond the scope of this paper and will be presented elsewhere.

Finally, it should be noted that, in theory, an arbitrary reference spectrum could be used in the $\beta\nu$ correlation. For example, when the $\beta\nu$ correlation analysis was performed using the spectrum collected at $t = 0$ as the reference spectrum, the absolute β_e values were shifted by approximately 60° (data not shown). However, the relative results were identical to those presented here. We chose to use the time-averaged spectrum exclusively as a reference spectrum in this paper to avoid further complicating the interpretation of the correlation results.

Conclusions

A modified 2D IR correlation method called $\beta\nu$ correlation analysis was introduced, which involves the cross correlation of IR band intensity variations with a purely mathematical function, which in this case is a simple sine function. When a model describing rates of change in intensities is considered, $\beta\nu$ correlation analysis can quantitatively determine the relative rates of intensity change and the degree of coherence between intensity variations in a discrete set of dynamic spectra. The result of the $\beta\nu$ correlation analysis is the calculation of a new parameter, the effective phase angle, or β_e. A specific model, the 'intensity change' model, was presented as a basis for interpreting β_e values. The level of uncertainty in the β_e values was considered for a set of simulated time-resolved spectra, which contains overlapping bands. An application of $\beta\nu$ correlation analysis to the solid$-$solid-phase transition (the "rotator" transition) of *n*-nonadecane was presented.

Acknowledgment. We would like to thank Professor Yukihiro Ozaki and Dr. Yan Wang of Kwansei-Gakuin University, Nishinomiya, Japan for providing us with their Array Basic program used to calculate the 2D IR spectra. This work was supported by the U.S. Public Health Service through National Institutes of Health Grant No. GM40117 (R.A.D.).

References and Notes

(1) Noda, I. *Appl. Spectrosc.* **1990**, *44*, 550−554.
(2) Marcott, C.; Noda, I.; Dowrey, A. E. *Anal. Chim. Acta* **1991**, *250*, 131−143.
(3) Noda, I. *Appl. Spectrosc.* **1993**, *47*, 1329−1336.
(4) Harrington, P. D.; Urbas, A.; Tandler, P. J. *Chemom. Intell. Lab. Syst.* **2000**, *50*, 149−174.
(5) Noda, I.; Dowrey, A. E.; Marcott, C.; Story, G. M.; Ozaki, Y. *Appl. Spectrosc.* **2000**, *54*, 236A−248A.
(6) Gadaleta, S. J.; Gericke, A.; Boskey, A.; Mendelsohn, R. *Biospectrosc.* **1996**, *2*, 353−364.
(7) Nabet, A.; Pezolet, M. *Appl. Spectrosc.* **1997**, *51*, 466−469.
(8) Noda, I.; Story, G. M.; Marcott, C. *Vib. Spectrosc.* **1999**, *19*, 461−465.
(9) Magtoto, N. P.; Sefara, N. L.; Richardson, H. H. *Appl. Spectrosc.* **1999**, *53*, 178−183.
(10) Hinterstoisser, B.; Salmen, L. *Vib. Spectrosc.* **2000**, *22*, 111−118.
(11) Elmore, D. L.; Dluhy, R. A. *Appl. Spectrosc.* **2000**, *54*, 956−962.
(12) Sonoyama, M.; Shoda, K.; Katagiri, G.; Ishida, H. *Appl. Spectrosc.* **1996**, *50*, 377−381.
(13) Ozaki, Y.; Liu, Y.; Noda, I. *Appl. Spectrosc.* **1997**, *51*, 526−535.
(14) Ren, Y. Z.; Shimoyama, M.; Ninomiya, T.; Matsukawa, K.; Inoue, H.; Noda, I.; Ozaki, Y. *Appl. Spectrosc.* **1999**, *53*, 919−926.
(15) Wu, P.; Siesler, H. W. *J. Mol. Struct.* **2000**, *521*, 37−47.
(16) Noda, I.; Lui, Y. L.; Ozaki, Y. *J. Phys. Chem.* **1996**, *100*, 8665−8673.
(17) McClure, W. F.; Maeda, H.; Dong, J.; Liu, Y.; Ozaki, Y. *Appl. Spectrosc.* **1996**, *50*, 467−475.
(18) Czarnecki, M. A.; Wu, P.; W. S., H. *Chem. Phys. Lett.* **1998**, *283*, 326−332.
(19) Pancoska, P.; Kubelka, J.; Keiderling, T. A. *Appl. Spectrosc.* **1999**, *53*, 655−665.

(20) Palmer, R. A.; Manning, C. J.; Chao, J. L.; Noda, I.; Dowrey, A. E.; Marcott, C. *Appl. Spectrosc.* **1991**, *45*, 12−17.

(21) Chazalviel, J. N.; Dubin, V. M.; Mandal, K. C.; Ozanam, F. *Appl. Spectrosc.* **1993**, *47*, 1411−1416.

(22) Ekgasit, S.; Ishida, H. *Appl. Spectrosc.* **1995**, *49*, 1243−1253.

(23) Shah, H. V.; Manning, C. J.; Arbuckle, G. A. *Appl. Spectrosc.* **1999**, *53*, 1542−1550.

(24) Wang, Y.; Lehmann, S. *Appl. Spectrosc.* **1999**, *53*, 914−918.

(25) Sonoyama, M.; Miyazawa, M.; Katagiri, G.; Ishida, H. *Appl. Spectrosc.* **1997**, *51*, 545−547.

(26) Mueller, M.; Buchet, R.; Fringeli, U. P. *J. Phys. Chem.* **1996**, *100*, 10 810−10 825.

(27) Buchet, R.; Wu, Y.; Lachenal, G.; Raimbault, C.; Ozaki, Y. *Appl. Spectrosc.* **2001**, *55*, 155−162.

(28) Noda, I. *Appl. Spectrosc.* **2000**, *54*, 994−999.

(29) Tandler, P. J.; Harrington, P. D.; Richardson, H. *Anal. Chim. Acta* **1998**, *368*, 45−57.

(30) Snyder, R. G.; Maroncelli, M.; Qi, S. P.; Strauss, H. L. *Science* **1981**, *214*, 188−190.

(31) Zerbi, G.; Magni, R.; Gussoni, M.; Moritz, K. H.; Bigotto, A.; Dirlikov, S. *J. Chem. Phys.* **1981**, *75*, 3175−3194.

(32) Casal, H. L.; Cameron, D. G.; Mantsch, H. H. *Can. J. Chem.* **1982**, *61*, 1, 1736−1742.

(33) Snyder, R. G. *J. Chem. Phys.* **1967**, *47*, 1316−1360.

(34) Maroncelli, M.; Qi, S. P.; Strauss, H. L.; Snyder, R. G. *J. Am. Chem. Soc.* **1982**, *104*, 6237−6247.

(35) Zerbi, G.; Magni, R.; Gussoni, M. *J. Mol. Struct.* **1981**, *73*, 235−237.

(36) Zerbi, G. *Adv. Chem. Series* **1983**, *203*, 487−531.

(37) Snyder, R. G. *J. Chem. Phys.* **1979**, *71*, 3229−3235.

(38) Jona, P.; Bassetti, B.; Benza, V.; Zerbi, G. *J. Chem. Phys.* **1987**, *86*, 1561−1567.